Lens-Based High-Sensitivity 5G mm-Wave Electromagnetic Field Sensors

Leila Gottmer[#], Huasheng Zhang[$], Nuria Llombart[$], Marco Spirito[#]
[#]Electronics Research Laboratory, Department of Microelectronics, Delft University of Technology, The Netherlands
[$] Terahertz Sensing Group, Department of Microelectronics, Delft University of Technology, The Netherlands
a.l.gottmer@tudelft.nl

***Abstract* — In this work, we present the development of a low-power and high-sensitivity electromagnetic field (EMF) sensor operating in the n258 FR2 band. The design of the sensor architecture and its sub-systems are discussed, and the sensor performance is characterised using over-the-air measurements. For the front end, a dual-polarised leaky-wave antenna feed is coupled to a dielectric lens and implemented in a multilayer PCB stack. The elliptical lens is 3D-printed using commercially available ABS. The back-end RF electronics are integrated on the same PCB to realise low-power direct down conversion sensing. The components include low noise amplifiers (LNA), digital step attenuators (DSA) and root-mean-square (RMS) detectors. An onboard 12-bit digitiser provides signal quantisation. The measured radiation patterns of the lens antenna agree well with the simulations with $17.18\,\mathrm{dBi}$ directivity. The responsivity is $-57.7\,\mathrm{dBm}$ and the power consumption is about $0.6\,\mathrm{W}$ for a single polarisation.**

***Keywords* — RF-EMF sensor, leaky-wave feed, lens antenna, RMS sensor, mm-wave, 5G.**

I. Introduction

The continuously growing demand for high data rates has been one of the targets in the development of fifth-generation (5G) telecommunication systems. To enable these systems to support increased peak data rates, additional available spectrum was granted globally [1]. Given the congested FR1 band, 5G systems have envisioned for the first time the inclusion of carrier frequencies in the mm-wave region [1]. The complex resource allocation and spatial multiplexing introduced by these systems have made it more challenging to characterise radio frequency electromagnetic fields (RF-EMF), especially those generated in congested locations, such as urban environments. Currently, maximum power extrapolation (MPE) procedures [2], scaled by stochastic correction factors, are used to characterise the EMF exposure of 5G New Radio (5G-NR) systems. Nevertheless, the novelties and complexities these systems introduce continue to contribute to public uncertainty and anxiety regarding the acceptance of 5G systems. Extensive development of low-cost R&D sensors for continuous RF-EMF monitoring has been generated recently [3]. Although several solutions are available in the sub $6\,\mathrm{GHz}$ range, very few solutions providing both low-cost and high sensitivity are currently available in the FR2 range.

Currently, most sensors use simple tri-axial antenna structures using dipoles [4] capable of achieving a near isotropic response at the expense of system dynamic range due to interfacing cable losses and lack of antenna gain, thus resulting in reduced system sensitivity. In this paper, we propose a lens-based dual-polarised sensor capable of continuously measuring RF-EMF in the n258 FR2 frequency band (i.e., the band ranging from $24.25\,\mathrm{GHz}$ to $27.50\,\mathrm{GHz}$). The sensor front-end is a high-gain lens antenna fed by a dual-polarised leaky-wave antenna (LWA). The lens is 3D printed, and the feed is implemented in a multilayer PCB stack with an integrated back cavity, enabling low-cost implementation. The simulated antenna S-parameters show $-10\,\mathrm{dB}$ over the n258 FR2 band for both polarisations and less than $-50\,\mathrm{dB}$ mutual coupling between the polarisations. Lastly, The radiation properties and sensor responsivity are characterised using over-the-air (OTA) measurements, and the overall sensor responsivity is $-57.5\,\mathrm{dBm}$.

II. Sensor Architecture

The proposed sensor is based on a RMS direct power detection topology. The simplified block scheme of the proposed architecture, with the 3D impression of the two main sub-blocks, is shown in Fig. 1.

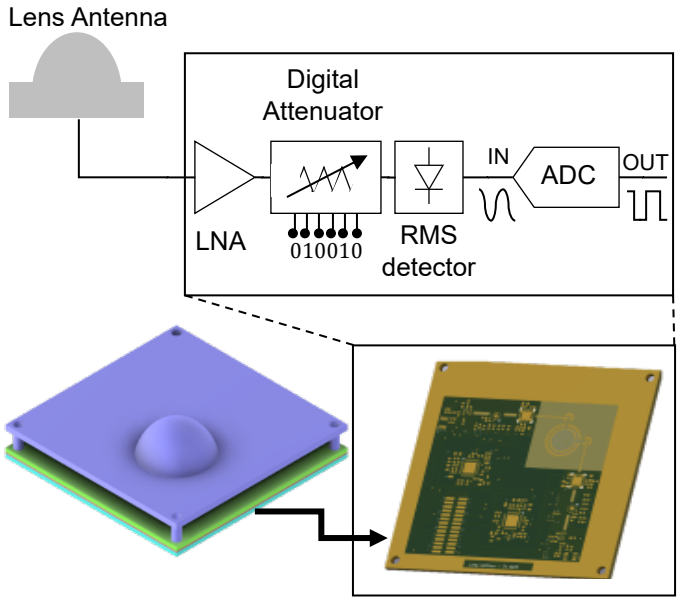

Fig. 1. Top level overview of the sensor node with the lens antenna in the RF front-end and the LNA, DSA, RMS detector and ADC in the RF back-end.

The front-end antenna interface is realised by a dual polarised lens antenna (detailed in Section II-A). A low noise

amplifier (LNA) paired with a digital step attenuator (DSA) provides the RMS detector output, which is directly digitised on the board by a fast digitiser (detailed in Section II-B).

A. *Lens Antenna Prototyping*

The front-end antenna should allow low-cost realisation and provide dual polarisation. The latter allows us to obtain the total power density independent of base station unit misalignment. Moreover, a higher antenna gain (compared to commercial tri-axial antennas [4]) in combination with the LNA/DSA architecture is chosen to improve the sensor sensitivity. Finally, low side lobe levels (SLLs) are targeted, given their critical impact when combining these sensors in (non-coherent) array topologies.

To achieve the aforementioned requirements, the lens antenna topology presented in [5] was chosen. In this work, the central frequency is adapted to 26.5 GHz to comply with the n258 FR2 band. The lens feed is an LWA [6], which consists of a resonant air cavity illuminated by dual polarised crossed slots coupled to crossed dipoles. This feed is implemented in a multilayer PCB stack, and the antenna dimensions are designed to optimise the matching performance in the FR2 band. The simulated S-parameters are shown in Fig. 2. The reflection coefficients of both ports (polarisations) are below -10 dB over the entire n258 FR2 band. Moreover, the mutual coupling between the two polarisations over this same band is below -50 dB. Note that the simulations in Fig. 2 do not include any ohmic losses. Instead, they were simulated separately, and the resulting loss contribution for both ports varies from 0.5 dB to 1 dB in the band of interest.

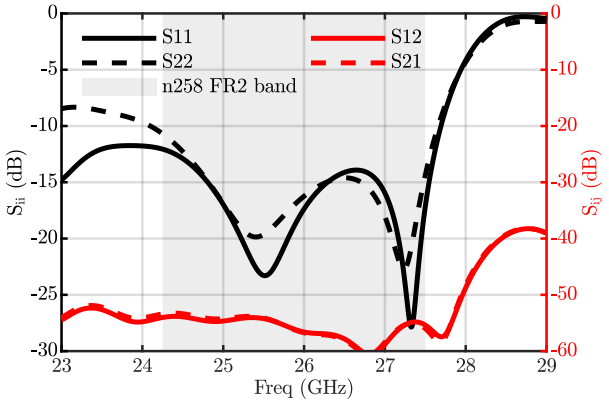

Fig. 2. S-parameters of the optimised LWA feed when radiating towards the semi-infinite medium of ε_r = 2.4. Note that the ohmic losses are not included. The grey region is the n258 FR2 band.

The LWA feed illuminates an elliptical dielectric lens through a resonant air cavity. A 3D design of the lens assembly is shown in Fig. 1. To reduce fabrication costs, the lens is realised using 3D printing technologies. The material used is ABS plastic, with a relative permittivity (ε_r) of 2.4 and a loss tangent ($\tan\delta$) of 5e-3 [7]. The dielectric loss in the lens is around 0.25 dB. The production of this prototype was realised using an Ultimaker S5. An infill density of 100 % was chosen in addition to an extra fine print resolution of 60 µm, leading to a fabrication time of 2 hours and 51 minutes. The fabricated lens and its assembly with the PCB feed is shown in Fig. 3.

(a) (b)

Fig. 3. (a) A side view of the assembled sensor showing the 3D printed dielectric lens with a truncation angle (θ_l) of 36° and an extension thickness (h_{top}) of 1.92 mm. (b) The assembled sensor placed on $\frac{\lambda}{2}$ (at 26.5 GHz) extensions to create the air cavity between the feed and the lens.

B. *Back-end electronics and PCB integration*

The integration of the RF back-end electronics on the bottom of the PCB is shown in Fig. 4. The components are detailed for one line-up, as shown in the inset of Fig. 4. The board contains a Qorvo QPA2628 LNA, the ADRF5731

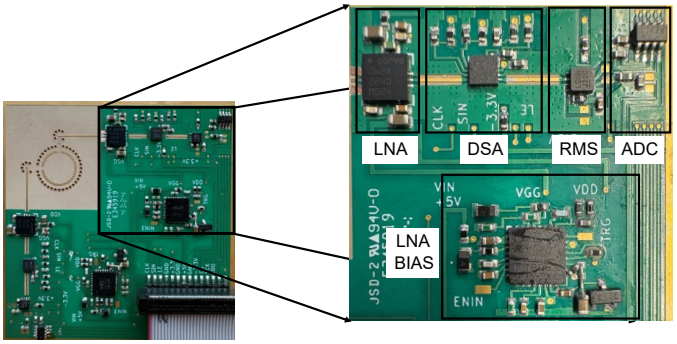

Fig. 4. RF back-end line-up showing the LNA, the DSA, the RMS detector and the ADC. Additionally, the circuitry for the LNA bias is shown as well.

DSA, an LTC5596 RMS detector, and a 12-bit LTC2312-12 ADC. The HMC920LP5E active bias controller biases the LNA. Furthermore, an external supply board provides the bias to all sensor board components. The combination of the LNA and DSA provide an extended dynamic range (DR) of 58 dB when compared to the 38 dB of the RMS detector. Furthermore, the noise floor level of the electronics is improved to approximately -60 dBm from the -38 dBm of the RMS detector topology. Table 1 shows the supply current, supply voltage and power consumption for each component of the line-up. Note that this table shows the data for a single line-up. The total estimated power consumption of one line-up is 0.60 W.

III. Sensor Measurements

In our first measurement campaign, the performance of the developed sensor is characterised using OTA setup shown Fig. 5. The sensor operates as a receiver, and its outputs are DC voltages from the back-end electronics. Two aspects of performance are measured. One is the radiation patterns of the front-end lens antenna; the other is the responsivity of the entire sensor.

Table 1. Estimated power consumption for one single line-up based on the datasheet information.

	Supply current mA	Supply voltage V	Power consumption mW
LNA	90	3.5	315
DSA	0.23	3.3	0.77
RMS	30	3.3	99
ADC	2.9	3.3	9.6
LNA Bias	35	5	175
Total			599.4

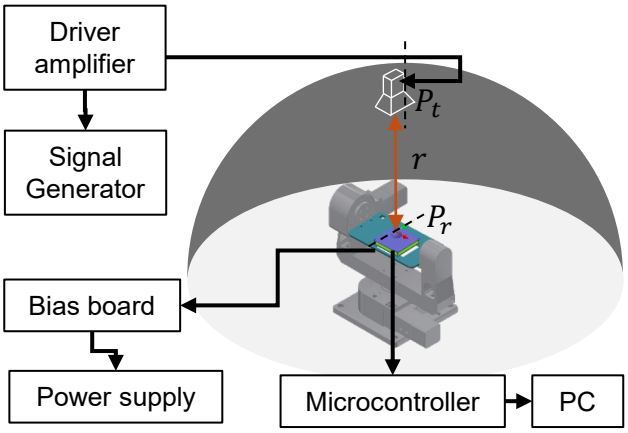

Fig. 5. A sketch of the measurement setup with the transmitting horn, the sensor node that is mounted on the gimbal and the connections to the other components.

In the setup, the transmitter is a WR28 pyramidal horn antenna from Eravant. The horn is installed on the top of a spherical dome and is connected to a WR-28 waveguide-to-coaxial adapter. An R&S SMA100B signal generator feeds the horn. Furthermore, a Mini-Circuits ZVA-02443HP+ wideband driver amplifier is placed at the transmitter side to extend the dynamic range. On the receiving side the sensor is mounted on a gimbal capable of rotating with two degrees of freedom. Moreover, the STM32 Nucleo microcontroller, which is used to set the attenuation levels and to read out the DC voltages of the ADC, connects to the sensor. The distance (r) between the horn aperture and the lens antenna aperture is approximately $60\,\mathrm{cm}$; therefore, both antennas can be considered in the far-field of each other.

In the following subsections, the measurement procedure and experimental results are detailed.

A. *Antenna radiation performance*

The radiation patterns of the lens antenna are measured first. Since they are independent of the incident power, the power level of the horn is fixed at $4.2\,\mathrm{dBm}$, which corresponds to a $-25\,\mathrm{dBm}$ power level of the signal generator. The lens antenna is rotated with the gimbal every 1° in elevation along two main planes. Normalised radiation patterns can be obtained by normalising the received voltage at each angle to the voltage at broadside, and by using the RMS conversion factor of $29\,\mathrm{mV\,dB^{-1}}$, the normalised radiation patterns can be obtained. Fig. 6 compares the radiation patterns at $26.5\,\mathrm{GHz}$ between simulations and measurements. The agreement is very good along both planes. Slight asymmetry in the measured main beam is associated with the limited fabrication accuracy of the 3D printer. The deviation in the side lobes can be attributed to the reflections caused by the measurement setup. From these patterns, we can roughly estimate the antenna directivity (by interpolating the two cuts to the whole azimuth angles). The measured directivity is $17.18\,\mathrm{dBi}$, which is very close to the simulated directivity of $17.05\,\mathrm{dBi}$.

Since the lens antenna is a receiver coupled to the electronics, the antenna gain cannot be directly measured using the Friis equation in the current measurement setup. Therefore, the following section uses simulated antenna gain to obtain the sensor responsivity. In a future measurement campaign, the gain will be characterised using a probe landing method.

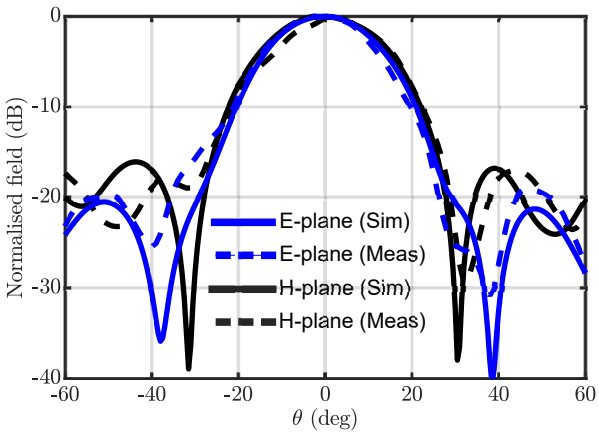

Fig. 6. Radiation patterns of the simulated and measured lens antenna in both the E- and H-plane.

B. *Sensor responsivity*

The responsivity of the sensor is defined as the received power P_r versus the DC output voltage. According to Friis equation, P_r can be obtained if the transmitted power (P_t), the gain of the transmitter (G_t), the gain of the receiver (G_r), and the distance between the two antennas are known. In this work, G_t = 15.79 dB, G_r = 15.8 dB (simulated gain) and the distance is $60\,\mathrm{cm}$. P_t is found by performing a reference plane translation from the signal generator to the input of the horn antenna.

In our OTA measurement setup, both the horn and sensor are fixed at broadside. The response curve is obtained by sweeping the RF input power levels and attenuation levels. The measurement results at $26.5\,\mathrm{GHz}$ are shown in Fig. 7.

It can be seen that in the linear region, the power-to-voltage conversion is as expected from the RMS detector datasheet. The grey region in the curve identifies the compression region of the driver amplifier used in this measurement. The deviation from the linear behaviour in the low power region of the $0\,\mathrm{dB}$ (the blue line in Fig. 7) can be attributed to the detector measuring the spurious content from the signal generator.

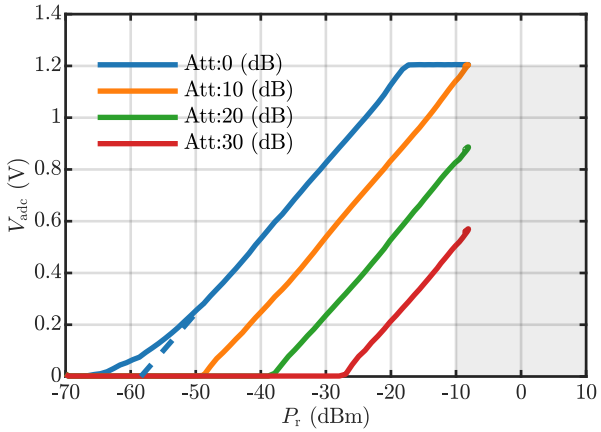

Fig. 7. The received power versus the voltage measured by the ADC for the four different attenuation levels, with the grey area denoting the compression region of the driver amplifier. The dashed line is the linear extrapolation of the 0 dB curve.

Therefore, the actual estimated sensitivity level is found by linearly extrapolating the 0 dB curve (as denoted by the dashed line in Fig. 7). Based on this curve, the expected sensitivity level is found to be $-57.7\,\mathrm{dBm}$, resulting in an average power density (S_{avg}) of $4.4 \times 10^{-6}\,\mathrm{W\,m^{-2}}$, or equivalently a field strength amplitude ($|E|$) of $0.058\,\mathrm{V\,m^{-1}}$.

IV. Conclusion

In this work, a low-power, high-sensitivity EMF sensor operating in the n258 FR2 band was presented. An LWA feed consisting of dual-polarised crossed slots coupled to crossed dipoles was implemented in a multilayer PCB stack. The design showed a simulated matching performance better than $-10\,\mathrm{dB}$ and a mutual coupling level below $-50\,\mathrm{dB}$. The dielectric lens fabrication was realised using 3D printing technologies. Furthermore, the RF back-end electronics, integrated on the bottom of the PCB, allowed for an extended DR of $58\,\mathrm{dB}$ and an improved noise floor level of $-57.7\,\mathrm{dBm}$. The radiation properties and responsivity were measured in an OTA characterisation. The radiation patterns show good agreement between the simulations and the measurement, with the directivity being $17.05\,\mathrm{dBi}$ and $17.18\,\mathrm{dBi}$, respectively. The estimated sensitivity level is $-57.5\,\mathrm{dBm}$. This value corresponds to an average power density of $4.4\times10^{-6}\,\mathrm{W\,m^{-2}}$, or equivalently, a field strength of $0.058\,\mathrm{V\,m^{-1}}$. In conclusion, the developed sensor shows promising results in terms of directivity and sensitivity to be employed in real-life RF-EMF measurement campaigns.

Acknowledgment

This work is part of the European Union's Horizon Europe research and innovation program under grant agreement No 101057527 (NextGEM). Funded by the European Union. Views and opinions expressed are however those of the authors only and do not necessarily reflect those of the European Union. Neither the European Union nor the granting authority can be held responsible for them.

References

[1] E. Hajlaoui, A. Zaier, A. Khlifi, J. Ghodhbane, M. B. Hamed, and L. Sbita, "4g and 5g technologies: A comparative study," in *2020 5th International Conference on Advanced Technologies for Signal and Image Processing (ATSIP)*, 2020, pp. 1–6. DOI: 10.1109/ATSIP49331.2020.9231605.

[2] M. D. Migliore, D. Franci, S. Pavoncello, *et al.*, "A new paradigm in 5g maximum power extrapolation for human exposure assessment: Forcing gnb traffic toward the measurement equipment," *IEEE Access*, vol. 9, pp. 101 946–101 958, 2021. DOI: 10.1109/access.2021.3092704. [Online]. Available: https://doi.org/10.1109/access.2021.3092704.

[3] E. Korkmaz, S. Aerts, R. Coesoij, *et al.*, "A comprehensive review of 5g nr rf-emf exposure assessment technologies: Fundamentals, advancements, challenges, niches, and implications," *Environmental Research*, vol. 260, p. 119 524, 2024, ISSN: 0013-9351. DOI: https://doi.org/10.1016/j.envres.2024.119524. [Online]. Available: https://www.sciencedirect.com/science/article/pii/S0013935124014294.

[4] N. products, *Products emf - broadband measuring devices nbm probes*. [Online]. Available: https://www.narda-sts.com/en/products/emf-broadband-measuring-devices/nbm-probes/.

[5] H. Zhang, S. Bosma, A. Neto, and N. Llombart, "A dual-polarized 27 dbi scanning lens phased array antenna for 5g point-to-point communications," *IEEE Trans. Antennas Propag.*, vol. 69, no. 9, pp. 5640–5652, 2021.

[6] N. Llombart, G. Chattopadhyay, A. Skalare, and I. Mehdi, "Novel terahertz antenna based on a silicon lens fed by a leaky wave enhanced waveguide," *IEEE Trans. Antennas Propag.*, vol. 59, no. 6, pp. 2160–2168, 2011.

[7] T. Whittaker, S. Zhang, A. Powell, C. Stevens, J. Y. Vardaxoglou, and W. Whittow, "3d printing materials and techniques for antennas and metamaterials: A survey of the latest advances," *IEEE Antennas and Propagation Magazine*, vol. PP, pp. 2–12, Jan. 2022. DOI: 10.1109/MAP.2022.3229298.